Boundary elements for modelling gravitational signals observed by inter-satellite ranging

Markus Antoni[1], **Matthias Weigelt**[2], **Wolfgang Keller**[1], **Tonie van Dam**[2]

[1]Universität Stuttgart, Geodätisches Institut, Stuttgart, Deutschland

[2]Université Du Luxembourg, Faculté des Sciences, de la Technologie et de la Communication, Luxembourg

antoni@gis.uni-stuttgart.de

Abstract

The recovery of the Earth's gravity field on a global scale is mainly based on satellite data, in particular the tracking of positions and velocities. The global behaviour of the gravity field is derived from the energy balance approach and analyzed by spherical harmonics.
In the region of interest, potential differences are created from range observations to achieve a higher spatial resolution. The remaining signal is modeled by triangular boundary elements and the results are converted into potential.
The residuals demonstrate the benefit of this combination of base functions, but also some challenges for further studies.

1. Boundary Elements

As the gravity field can only be observed on the surface and the outer space, the inhomogenous mass distribution can be compressed to a single layer in the modelling. The potential V of the layer on the surface is described by

$$V(\vec{x}) = G \iint_{\mho} \frac{\sigma(\vec{X}_Q(\lambda,\vartheta))}{\|\vec{x} - \vec{X}_Q(\lambda,\vartheta)\|} \mathrm{d}\vec{X}_Q(\lambda,\vartheta) \tag{1}$$

with

- G: gravitational constant
- σ: surface density
- (λ, ϑ): longitude and co-latitude
- $\vec{x}$: position of interest
- $\vec{X}_Q$: location on the surface $\mho$.

In the approach of boundary elements, the surface is subdivided into I simpler geometries like rectangular patches or – in our case – triangles.
Each triangle is defined by **nodes** located at the corners $(k = 1, 2, 3)$, where the density values $\sigma_{i,k}$ are estimated in the adjustment. Apart from that, a 'rule' for interpolating the density values is required, which is denoted as **shape function** $\Phi_{i,k}$.
Figure 1 shows the triangles for the regional improvement of this study, where the initial grid is generated by an iterative sub-division of an icosaedron. The color in the nodes represent the density values based on the potential differences.

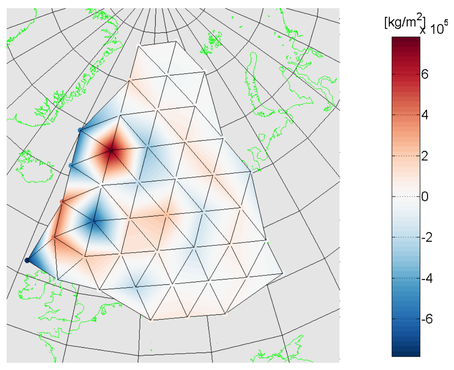

Figure 1: *Triangulation in the region of interest*

In the implementation, the triangles are transformed by the Jacobian matrix $\mathbf{J}_i(\xi, \eta)$ to the normal triangle with the local coordinates (ξ, η) and the nodes $\{(-1,-1), (1,-1), (-1,1)\}$:

$$V = G \sum_{i=1}^{I} \sum_{k=1}^{K} \sigma_{i,k} \int_{-1}^{1} \int_{-1}^{-\xi} \frac{\mathbf{J}_i(\xi,\eta)\Phi_{i,k}(\xi,\eta)\sin\vartheta(\xi,\eta)}{\|\vec{x} - \vec{X}_Q(\lambda(\xi,\eta),\vartheta(\xi,\eta))\|} \mathrm{d}\xi\mathrm{d}\eta \tag{2}$$

The integrals per boundary element are solved by numerical quadrature with Gaussian evaluation points [2].

2. Modeling of SST-data

A GRACE-like scenario of 30 days is simulated with a constant rotation $\omega_E = 7.292115 \cdot 10^{-5} \frac{\mathrm{rad}}{\mathrm{s}}$ of the Earth and the Keplerian elements in Table 1.

	GRACE A	GRACE B
semi-major axis a	6791049 m	6789925 m
eccentricity e	0.00045	0.00044
inclination I	89.45°	89.45°
rectascension Ω	171.50°	171.50°
perigee ω	6.33°	−17.66°

Table 1: *Initial Keplerian elements of the simulation*

The gravity field of the orbit integration consists in spherical harmonic coefficients of the EIGEN model up to degree and order 30 and 4 rectangular patches of single mass layers in the area of interest. The latter one cause a disturbing potential of $\max|\delta T| \approx 1 \frac{\mathrm{m}^2}{\mathrm{s}^2}$ along the orbit.

3. Analysis

3.1 Spherical Harmonics

The global behaviour is recoverd via the **energy balance approach** applied on both satellites [3]:

$$T = \frac{1}{2}\|\dot{\vec{x}}_i\|^2 - \dot{\vec{x}}_i^{\top}(\vec{\omega} \times \vec{x}_i) - E_0 \tag{3}$$

- T potential along the orbit
- $\vec{x}_i$ position in the inertial frame
- $\vec{\omega} = (0, 0, \omega_E)$ rotation vector
- E_0 contstant of the integration

The global potential is modeled by a superposition of spherical harmonics up to degree 30

$$\hat{T}_{global} = \frac{GM}{R} \sum_{n=0}^{30} \left(\frac{R}{\|\vec{x}_i\|}\right)^{n+1} \sum_{m=0}^{n} \overline{P}_{nm}(\cos\vartheta) \cdot \left[\overline{C}_{nm}\cos m\lambda + \overline{S}_{nm}\sin m\lambda\right], \tag{4}$$

where the Stokes coefficients $\{\overline{C}_{nm}, \overline{S}_{nm}\}$ are estimated by least square adjustment together with the offset E_0.
For the further investigation, the data are restricted to a region of interest around the disturbing patches. By subtracting the spherical harmonic synthesis of the estimated coefficients from the energy balance, the residual potential along the orbit is achieved (cf. Figure 2). As the maximum is smaller than the known potential of the disturbing patches, parts of this signal are already modeled by the spherical harmonics!

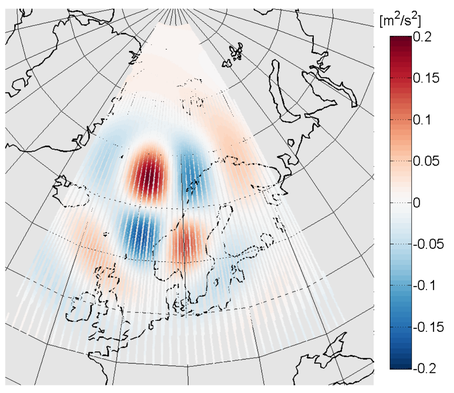

Figure 2: *Residual potential: energy balance minus potential of estimated coefficients*

3.2 Boundary elements

To increase the spatial resolution, the range-rate $\dot{\rho}$ of GRACE-like missions is introduced into the observation equation. Therefor, equation 3 is applied for both satellites – with the positions $\vec{x}_i$ respectively $\vec{y}_i$ – and subtracted from each other [1]:

$$T_{12} = \dot{\vec{x}}^{\top}\dot{\rho} + \frac{1}{2}\|\dot{\rho}\|^2 - \dot{\vec{y}}_i^{\top}(\vec{\omega} \times \vec{y}_i) + \dot{\vec{x}}_i^{\top}(\vec{\omega} \times \vec{x}_i) - \Delta E_0 \tag{5}$$

The **potential difference** T_{12} and the residuals after removing the potential of the boundary elements with estimated densities are shown in Figure 3 and 4 and Table 2.

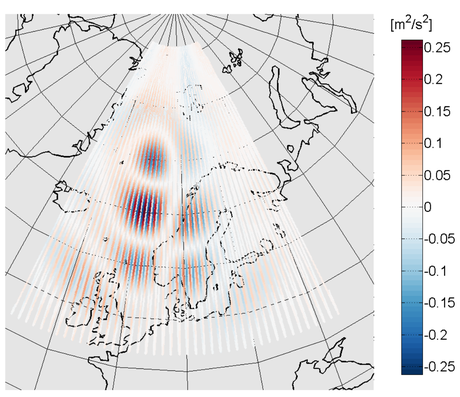

Figure 3: *Potential differences T_{12} based on satellite tracking*

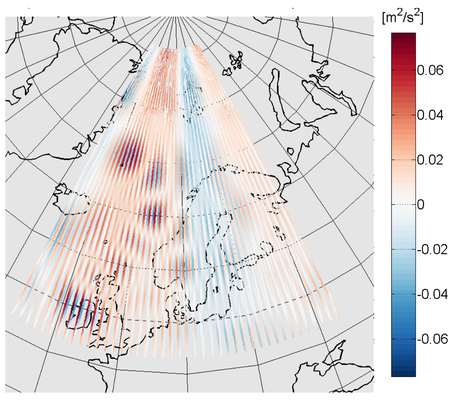

Figure 4: *Residuals of potential differences after removing the effect of the boundary elements*

	T_{12}	synthesis	difference
MEAN	$32.22 \cdot 10^{-3}$	$29.23 \cdot 10^{-3}$	$14.54 \cdot 10^{-3}$
MAX	$262.05 \cdot 10^{-3}$	$217.11 \cdot 10^{-3}$	$76.85 \cdot 10^{-3}$
MIN	0	$0.131 \cdot 10^{-6}$	$1.500 \cdot 10^{-6}$
STD	$35.54 \cdot 10^{-3}$	$33.19 \cdot 10^{-3}$	$11.59 \cdot 10^{-3}$

Table 2: *Statistic of the potential differences (correlation: 89%)*

As the true potential is known in the study, we can compare these values with the potential caused by the estimated spherical harmonic coefficients and the boundary elements. For a better visualization, the differences between the true field and the estimated reference $\hat{T}_{global}$ is considered in Figure 5 and Table 3.

	$T(true) - \hat{T}_{global}$	synthsis	difference
MEAN	$43.45 \cdot 10^{-3}$	$45.51 \cdot 10^{-3}$	$18.32 \cdot 10^{-3}$
MAX	$236.88 \cdot 10^{-3}$	$195.04 \cdot 10^{-3}$	$68.427 \cdot 10^{-3}$
MIN	$0.90152 \cdot 10^{-3}$	$18.835 \cdot 10^{-6}$	$0.35980 \cdot 10^{-6}$
STD	$31.60 \cdot 10^{-3}$	$29.49 \cdot 10^{-3}$	$15.72 \cdot 10^{-3}$

Table 3: *Statistic of the true potential and the reconstruction (correlation: 75%)*

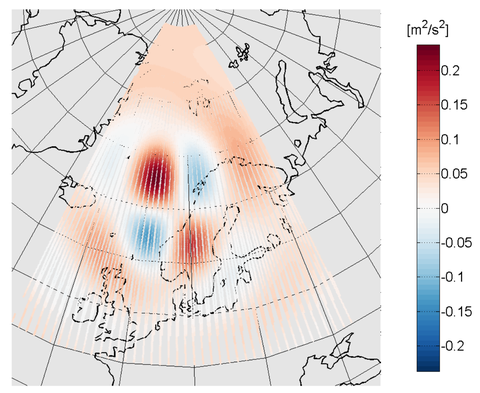

Figure 5: *True signal caused by the spherical harmonic coefficients of the true field minus the estimated coefficients (almost equivalent to Figure 3 except of the integration constant)*

Figure 6 visualizes the residuals of the potential between the error of the spherical harmonics coefficients and the boundary elements. The structures in the residuals are almost in the size of the boundary elements and with a magnitude of one third of the resdiual signal. A higher degree for the spherical harmonics and adaptive triangles will avoid this systematic behaviour.

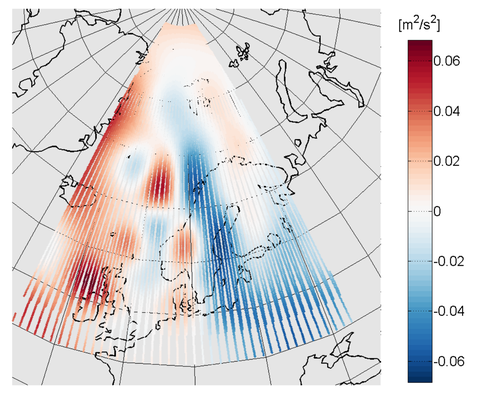

Figure 6: *Residuals of the true signal after removing the potential of the boundary elements*

4. Conclusion

The combination of energy balance approach and potential differences can reproduce the gravity field along the orbit only to a certain extend at the moment. Further improvements are expected by

- adaptive modifications of the nodes and size of the triangles,
- boundary elements with more nodes and a non-linear shape function,
- weighted adjustment of both kind observations,
- and tuning of maximum degree of spherical harmonics and the size of the boundary elements.

References

[1] C. Jekeli (1999): *The Determination of gravitational potential differences from staellite-to-satellite tracking.* Celestial Mechanics and Dynamical Astronomy 75:85-101

[2] M. Weigelt, W. Keller, and M. Antoni (2012): *On the Comparison of Radial Base Functions and Single Layer Density Representations in Local Gravity Field Modelling from Simulated Satellite Observations.* In: N. Sneeuw, P. Novák, M. Crespia and Fernando Sansò: *VII Hotine-Marussi Symposium on Mathematical Geodesy*, Vol. 137, pp 199-204

[3] M. Wermuth (2008): *Gravity Field Analysis from the Satellite Missions CHAMP and GOCE.* PhD, TU-München